Hindawi
International Journal of Antennas and Propagation
Volume 2019, Article ID 4923964, 16 pages
https://doi.org/10.1155/2019/4923964

Research Article

Compact Microwave Components with Harmonic Suppression Based on Artificial Transmission Lines

Wen Huang, Jia Li, Ping Li, and Xi Guo

College of Electronic Engineering, Chongqing University of Posts and Telecommunications, Chongqing 400065, China

Correspondence should be addressed to Wen Huang; huangwen@cqupt.edu.cn

Received 20 November 2018; Revised 4 February 2019; Accepted 28 February 2019; Published 2 May 2019

Academic Editor: Hervé Aubert

Copyright © 2019 Wen Huang et al. This is an open access article distributed under the Creative Commons Attribution License, which permits unrestricted use, distribution, and reproduction in any medium, provided the original work is properly cited.

In this paper, compact microwave components, including a Wilkinson power divider and a 3 dB branch-line coupler based on artificial transmission lines (ATLs) with harmonic suppression, are presented. A section ATL is consisted of microstrip stepped impedance transmission lines and a microstrip interdigital capacitor. To achieve a compact size, the stepped impedance transmission lines are folded into a right-angled triangle shape. For the ATL, the interdigital capacitor is used to suppress harmonics. By employing two sections of 70.7 Ω ATLs with a right-angled triangle shape to replace conventional transmission lines, the proposed power divider working at 0.9 GHz achieves a size miniaturization with the 58.8% area of a conventional case. In addition, the power divider has good harmonic suppression performance. In the design of a branch-line coupler, two pairs of ATLs with 50 Ω and 35.4 Ω are utilized. For 50 Ω ATLs, the ATLs are designed to a right-angled triangle shape. Meanwhile, to obtain a more compact size, these 35.4 Ω ATLs are modified to an isosceles trapezoid shape. The proposed branch-line coupler operating at 0.9 GHz accounts for merely 33.4% of a coupler adopting conventional microstrip transmission lines. Moreover, the harmonics of a branch-line coupler are suppressed effectively as well. Finally, measured results of the proposed Wilkinson power divider and branch-line coupler display good performance and agree with their simulated results well.

1. Introduction

The rapid development of the modern communication system makes a high requirement for size miniaturization of microwave components [1–3]. At present, size miniaturization methods of microwave components include loading lumped elements [4], using right/left-handed transmission lines [5], employing a defected ground structure (DGS) [6], utilizing a microstrip electromagnetic bandgap (EBG) [7], and applying slow-wave transmission lines with inductive and capacitive loading [8]. In these miniaturization methods, using artificial transmission lines (ATLs) is a good solution due to a flexible design and easy fabrication on a printed circuit broad. Besides, harmonic suppression can improve the signal-to-noise ratio of the communication system, which is also a hot research spot for microwave components. To achieve harmonic suppression, these methods are proved to be effective, such as using an ultra-wideband band-stop filter [9], an electromagnetic bandgap [10], open stubs [11], a defected ground structure [12], and inductively loaded slow-wave transmission lines [13].

The Wilkinson power divider, which works as a divider and combiner of power, is extensively used in a feed network for an antenna [14]. The conventional Wilkinson power divider consists of two sections of 70.7 Ω quarter-wavelength transmission lines and an insolation resistor. Therefore, the size of the Wilkinson power divider is mainly determined by the size of quarter-wavelength transmission lines at operating frequency, which results in a large occupied area, especially when operating at low frequency. Besides, the conventional Wilkinson power divider realized by microstrip lines cannot suppress harmonics. Therefore, some miniaturization methods of Wilkinson power dividers are reported, such as using short circuited half-wavelength and quarter-wavelength resonators [15], loading coupled resonator topology [16], utilizing topology consisted of half-wavelength resonators and

quarter-wavelength resonators [17], and using open dual-transmission line stub and L-type artificial lowpass transmission line structures [18]. These power dividers mentioned above not only have an obvious reduced size but also have a good harmonic suppression performance. In [15], harmonic suppression is realized by using lowpass filters. In [16], a net-type resonator is designed to obtain rejection of harmonic responses. In [17], the mixed electric and magnetic coupling and cross-coupling between three quarter-wavelength resonators generate three transmission zeroes to suppress harmonics. In [18], open dual-transmission line stub, L-type artificial lowpass transmission lines, open stub, and extension line modules are designed to suppress harmonics. These power dividers mentioned above can achieve a compact size and good harmonic suppression, but -15 dB bandwidths of these cases are narrow, which are, respectively, only 2.4%, 4.5%, 6.5%, and 21.1%.

A branch-line coupler is another important microwave component used in a modern communication system. However, the conventional 3 dB branch-line coupler is also confronted with the problem of a large occupied area brought in by two pairs of quarter-wavelength transmission lines with 50 Ω and 35.4 Ω. In order to reduce the size, some solutions are reported, such as loading a π-equivalent artificial transmission line [19], using asymmetrical T-structures [20], utilizing high-impedance transmission lines and interdigitated shunt capacitors [21], applying artificial transmission line combined with meandered lines and resonators [22], and employing transmission lines loaded resonators [23]. However, only the couplers in [21–23] can realize harmonic suppression. In [21], the second-order harmonic is suppressed to 20 dB by using interdigitated shunt capacitors. In [22], shunt LC resonators generate suppression for high-frequency harmonics, but a second-order harmonic and third-order harmonic cannot be suppressed. In [23], harmonics are suppressed due to the transmission zeros of resonators. In addition, these cases in [19, 21] are realized with size reduction, but 15 dB bandwidths are only 8.9% and 7.2%. These methods are difficult to achieve a reduced size, good bandwidth, and harmonic suppression at the same time.

In this paper, a method of using ATLs for size miniaturization and harmonic suppression employed on the Wilkinson power divider and 3 dB branch-line coupler is presented. These ATLs consist of stepped impedance transmission lines and interdigital capacitors. In the design of ATLs, these stepped impedance lines are folded into a right-angled triangle shape or isosceles trapezoid shape for a more compact size. Then, the interdigital capacitor plays a function of harmonic suppression. Finally, the proposed Wilkinson power divider and branch-line coupler have similar bandwidths of 58.2% and 17% compared with conventional components, while a compact size and harmonic suppression are realized at the same time.

2. Theoretical Analysis of an ATL

2.1. Design Concepts. As shown in Figure 1(a), a section of the 70.7 Ω ATL with a right-angled triangle shape is composed of five sections of microstrip low-impedance transmission lines and six sections of microstrip high-impedance transmission lines. Additionally, there are two sections of uniform transmission lines connected to ports. The low-impedance lines and high-impedance lines are cascaded alternately and then folded into a right-angled triangle shape for a compact size. Meanwhile, an interdigital capacitor is placed in the middle of an ATL to suppress harmonics. The equivalent circuit of the 70.7 Ω ATL is given by Figure 1(b). Each uniform transmission line connected to a port can be equivalent to a series inductor L_{as1} and a shunt capacitor C_{as1} to ground. Correspondingly, the high-impedance lines can be equivalent to series inductors L_{as2}, L_{as3}, and L_{as4}, and these low-impedance lines work as equivalent shunt capacitors C_{as2}, C_{as3}, and C_{as4} to ground. The interdigital capacitor is placed between several high-impedance lines and between low-impedance lines, so it can be equivalent to several series capacitors in parallel and parasitic capacitors to ground. For the sake of simplicity, as marked in Figure 1(a), the microstrip interdigital capacitor is divided into two parts as interdigital A1 and interdigital A2 and then be equivalent to series capacitors C_{ap1} and C_{ap2}. Besides, the shunt capacitors C_{a11}, C_{a12}, C_{a21}, and C_{a22} represent parasitic capacitors of the interdigital capacitor.

For the equivalent circuit of the 70.7 Ω ATL, the total inductance of equivalent series inductors can be represented by L_{t1}, and the total capacitance of equivalent shunt capacitors can be presented by C_{t1}. And they can be given by

$$\begin{aligned} L_{t1} &= 2L_{as1} + 2L_{as2} + 2L_{as3} + 2L_{as4}, \\ C_{t1} &= 2C_{as1} + 2C_{as2} + 2C_{as3} + C_{as4} + C_{a11} + C_{a12} + C_{a21} + C_{a22}. \end{aligned} \tag{1}$$

In the design of the 3 dB branch-line coupler, 50 Ω and 35.4 Ω ATL are designed. For a 50 Ω ATL, the layout and its equivalent circuit are given by Figure 2. It has similar layout and equivalent circuit as a 70.7 Ω ATL. The total inductance L_{t2} of equivalent series inductors and total capacitance C_{t2} of equivalent shunt capacitors are calculated by

$$\begin{aligned} L_{t2} &= 2L_{bs1} + 2L_{bs2} + 2L_{bs3} + 2L_{bs4} + 2L_{bs5}, \\ C_{t2} &= 2C_{bs1} + 2C_{bs2} + 2C_{bs3} + C_{bs4} + C_{b11} + C_{b12} + C_{b21} + C_{b22}. \end{aligned} \tag{2}$$

The layout and equivalent circuit of the 35.4 Ω ATL are shown in Figure 3. The 35.4 Ω ATLs are modified to an isosceles trapezoid shape to realize a more compact size for the branch-line coupler. Referring to its layout, the 35.4 Ω ATL is comprised of three sections of low-impedance transmission lines and four sections of high-impedance transmission lines. The two transmission lines connected to ports can be equivalent to series inductor L_{cs1} and shunt capacitor C_{cs1} to ground. In order to analyze the interdigital capacitor more accurately, the

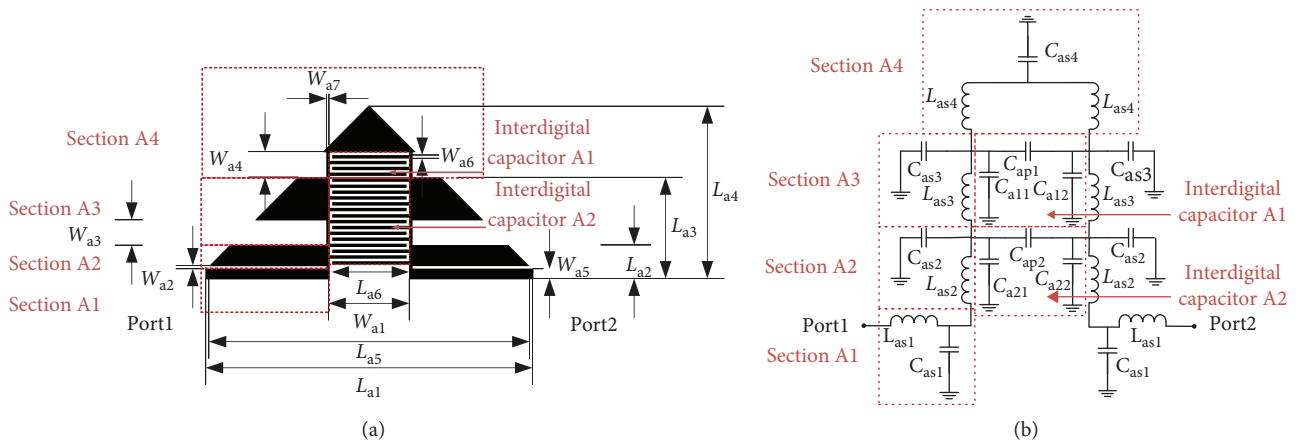

Figure 1: A section of 70.7 Ω ATL with a right-angled triangle shape: (a) layout and (b) equivalent circuit.

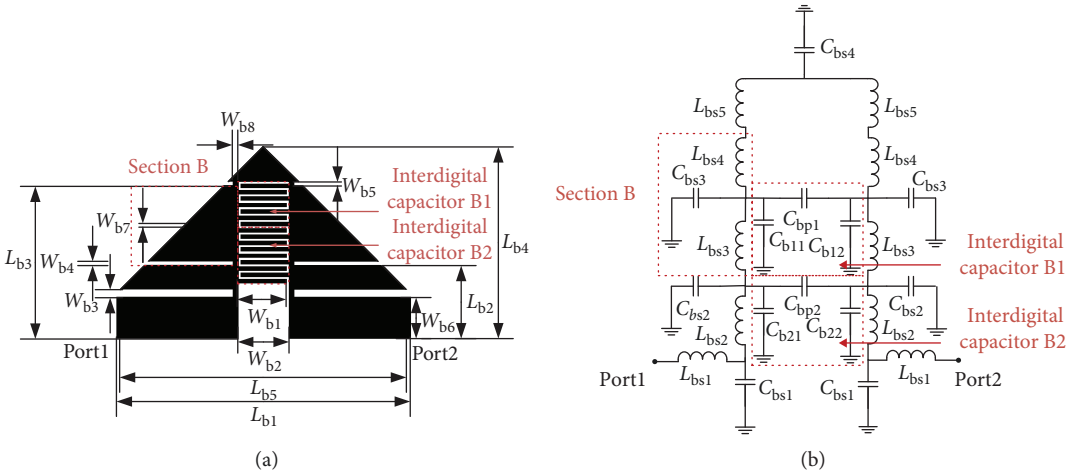

Figure 2: A section of 50 Ω ATL with a right-angled triangle shape: (a) layout and (b) equivalent circuit.

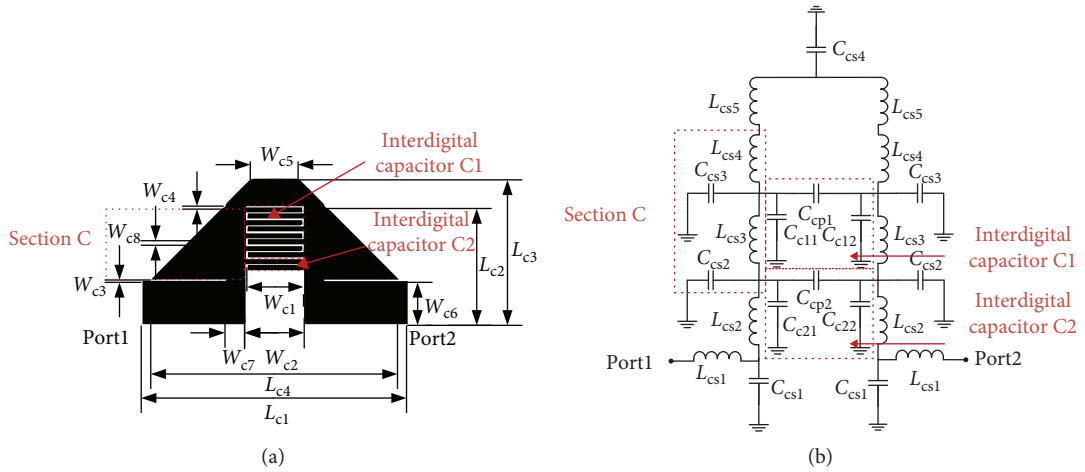

Figure 3: A section of 35.4 Ω ATL with an isosceles trapezoid shape: (a) layout and (b) equivalent circuit.

interdigital capacitor is divided into two parts. As marked in Figure 3(a), interdigital capacitor C1 and interdigital capacitor C2 can be equivalent to series capacitors C_{cp1} and C_{cp2} and parasitic capacitors C_{c11}, C_{c12}, C_{c21}, and C_{c22} to ground. The total series inductance L_{t3} and total shunt capacitance C_{t3} are given by

$$L_{t3} = 2L_{cs1} + 2L_{cs2} + 2L_{cs3} + 2L_{cs4} + 2L_{cs5},$$
$$C_{t3} = 2C_{cs1} + 2C_{cs2} + 2C_{cs3} + C_{cs4} + C_{c11} + C_{c12} + C_{c21} + C_{c22}. \quad (3)$$

According to the uniform transmission line theory, characteristic impedance Z_i ($i = 1,2,3$) and phase propagation constant β_i ($i = 1,2,3$) of per unit length are determined by $Z_i = \sqrt{L_i/C_i}$ and $\beta_i = \omega\sqrt{L_i \cdot C_i}$, where L_i and C_i are the inductance and capacitance per unit length along the transmission line and ω represents the operating angular frequency. For ununiform transmission lines such as ATLs, when the physical length of the ATL is less than one-eighth of a guided wavelength, the ununiform transmission lines can approximate to uniform transmission lines [24]. Then, for the ATL, $L_{ti} = L_i l_i$ and $C_{ti} = C_i l_i$, where L_{ti} and C_{ti} are the total series inductance and shunt capacitance and l_i is the physical length of a unit ATL. The characteristic impedance Z_i and electrical length θ_i of a unit of an ATL can be calculated as

$$Z_i = \sqrt{\frac{L_i}{C_i}} = \sqrt{\frac{L_{ti}}{C_{ti}}}, \quad (4)$$

$$\theta_i = \beta_i l_i = \omega\sqrt{L_i \cdot C_i} l_i = \omega\sqrt{L_{ti} \cdot C_{ti}}. \quad (5)$$

From formulas (4) and (5), we can find, for a unit ATL with the same length, if L_{ti} and C_{ti} increase proportionally, that Z_i would remain unchanged, while the electrical length θ_i would increase. In turn, with a given characteristic impedance Z_i and electrical length θ_i of a unit of an ATL, when L_i and C_i are increased proportionally, characteristic impedance Z_i would be unchanged, while phase propagation constant β_i of per unit length would be increased, so the required physical length l_i is significantly reduced.

For stepped impedance transmission lines, using the lines with high characteristic impedance is equivalent to loading more inductance per unit length, while employing the lines with low characteristic impedance is equivalent to loading more capacitance per unit length than conventional microstrip transmission lines. In the design of an ATL, stepped impedance transmission lines folded into a right-angled triangle shape would add more capacitance and inductance for per physical length, so the required physical length can be further reduced. In a practical design, the 35.4 Ω ATL is modified to an isosceles trapezoid shape to realize a more compact size of a branch-line coupler.

Owing to the impedance invariance of half wavelengths, conventional transmission lines including stepped impedance transmission lines have many harmonic pass-bands at multiples of central frequency. In order to suppress harmonics effectively, a microstrip interdigital capacitor is used in the ATL, which is equivalent to several series capacitors. These series capacitors are shunted with inductors, forming *LC* parallel-resonant circuits, as shown in Figures 1(b), 2(b), and 3(b). According to the stopband characteristic of *LC* parallel-resonant circuits at resonant frequency, these high-order harmonics at multiples of central frequency will be suppressed effectively by this way. Besides, the performance of harmonic suppression can be changed by changing the number and size of an interdigital capacitor's fingers. Finally, in order to realize a more compact structure of the proposed components using ATLs, each quarter-wavelength line is replaced by one unit ATL with 90°, though the optimum number of ATL units is proved to be two in [8, 13].

Based on the above analysis, taking the ATL with the required 70.7 Ω characteristic impedance and 90° electric length as an illustration, the design procedure of ATL can be described as follows:

Step 1. Based on the layout of an ATL just like that in Figure 1(a), create a rough model of an ATL in the software of IE3D. Obviously, the physical dimensions of each section in the model as shown in Figure 4 are arbitrary.

Step 2. The ATL is simulated by software of IE3D. The value of characteristic impedance Z_1 can be obtained by simulation directly, and electric length θ_1 can be got by simulated Ang(S_{21}).

Step 3. Compare the simulated characteristic impedance and electric length with the required goals. When required goals are not achieved, then, according to equations (4) and (5), decide the value of L_{t1} and C_{t1} should be increased or reduced.

In tuning of characteristic impedance Z_1, when the simulated characteristic impedance Z_1 is lower than 70.7 Ω, according to equation (4), we can increase total inductance L_{t1} or reduce total capacitance C_{t1}. When the simulated characteristic impedance Z_1 is higher than 70.7 Ω, we can reduce total inductance L_{t1} or increase total capacitance C_{t1}.

In tuning of electric length θ_1, when electric length θ_1 is smaller than 90°, according to equation (5), we can increase total inductance L_{t1} or total capacitance C_{t1}. When simulated electric length θ_1 is larger than 90°, we can reduce total inductance L_{t1} or total capacitance C_{t1}.

According to equation (1), changing the total inductance L_{t1} or total capacitance C_{t1} can be realized by changing the inductance and capacitance of each related section. For example, extending line length or reducing line width of these high-impedance lines can increase inductance of L_{as2}, L_{as3}, and L_{as4}, and reducing the area of low-impedance lines can reduce capacitance of C_{as2}, C_{as3}, and C_{as4} as shown in Figure 1(b).

So tuning physical dimensions of each section can change total inductance L_{t1} and total capacitance C_{t1}, to obtain the designed 70.7 Ω and 90°.

Step 4. Tune fingers of interdigital capacitors to adjust the performance of harmonic suppression, including frequency of transmission zero and range of stopband.

Step 5. To obtain equivalent inductance and capacitance of ATL to verify our design, with designated 70.7 Ω

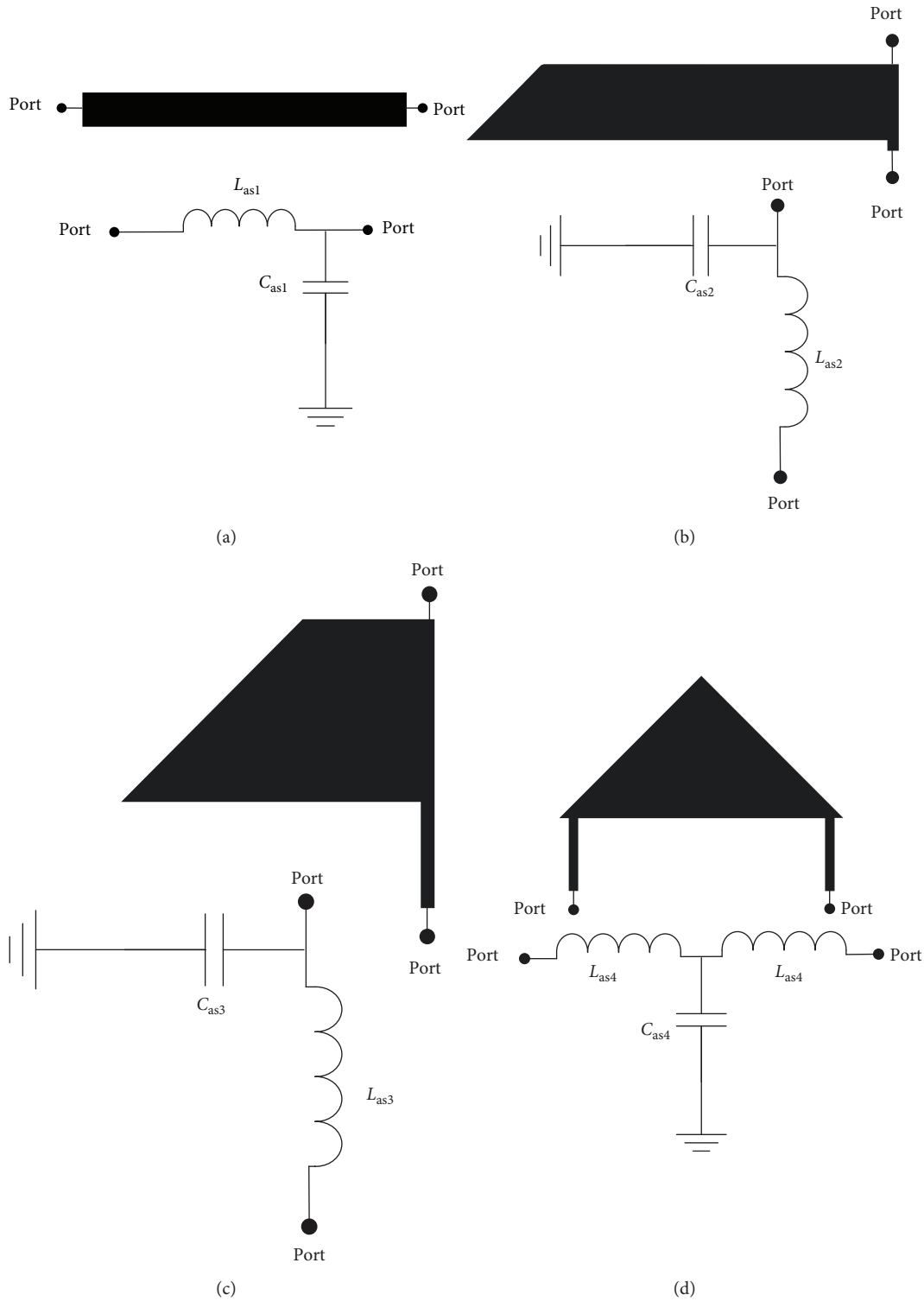

Figure 4: Continued.

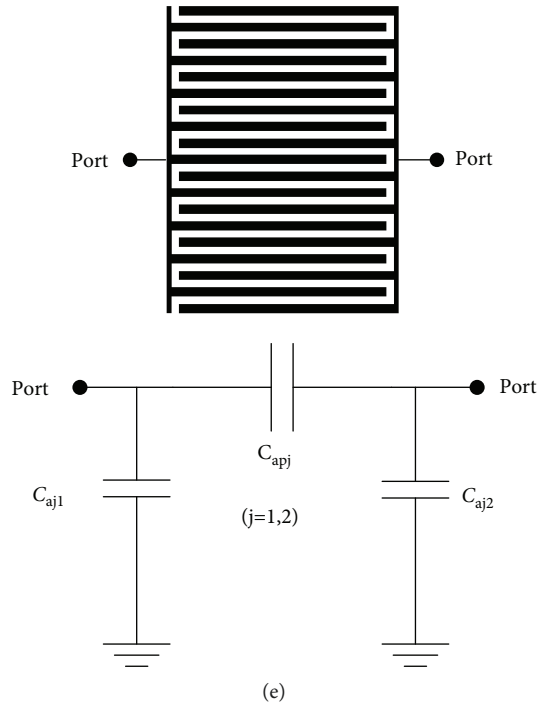

Figure 4: Each section of the 70.7 Ω ATL and their equivalent circuit: (a) section A1, (b) section A2, (c) section A3, (d) section A4, and (e) interdigital capacitor Aj ($j = 1, 2$).

characteristic impedance and 90° electric length, we use formulas (4) and (5) to obtain L_{t1} and C_{t1}.

Step 6. Each section as shown in Figure 4 is simulated by the simulation software of IE3D and converted to L-, T-, or π-equivalent circuit. And then parameter extraction of equivalent elements is based on impedance or admittance matrices.

2.2. Parameter Extraction. The process of parameter extraction is similar for the ATL of 70.7 Ω, 50 Ω, and 35.4 Ω, so we take the 70.7 Ω ATL as an example to analyze. In order to analyze the equivalent circuit of the 70.7 Ω ATL easily, the ATL is divided into several sections, as shown in Figure 1. Each section and their equivalent circuit are given in Figure 4. Obviously, a more accurate equivalent circuit can be achieved by dividing the ATL into more sections when analyzing the ATL. To extract the equivalent element values of each section, full-wave simulation software IE3D is applied to calculate impedance or admittance matrices from the corresponding equivalent circuits of each section.

The admittance matrix of the equivalent circuit for section A1 in Figure 4(a) is expressed as

$$\begin{bmatrix} Y_{11}^{A1} & Y_{12}^{A1} \\ Y_{21}^{A1} & Y_{22}^{A1} \end{bmatrix} = \begin{bmatrix} -\dfrac{j}{\omega L_{as1}} & \dfrac{j}{\omega L_{as1}} \\ \dfrac{j}{\omega L_{as1}} & j\omega C_{as1} - \dfrac{j}{\omega L_{as1}} \end{bmatrix}. \quad (6)$$

From the formula above, the equivalent value of elements can be obtained by

$$L_{as1} = \frac{1}{2\pi f_0 \operatorname{Im}\left(Y_{12}^{A1}\right)}, \qquad C_{as1} = \frac{\operatorname{Im}\left(Y_{22}^{A1}\right) + \operatorname{Im}\left(Y_{21}^{A1}\right)}{2\pi f_0}. \quad (7)$$

Due to similar L-type circuit, the equivalent value of elements in Figures 4(b) and 4(c) can be readily calculated based on the admittance matrix by the same way.

For section A4 in Figure 4(d), its impedance matrix can be given by

$$\begin{bmatrix} Z_{11}^{A4} & Z_{12}^{A4} \\ Z_{21}^{A4} & Z_{22}^{A4} \end{bmatrix} = \begin{bmatrix} j\omega L_{as4} - \dfrac{j}{\omega C_{as4}} & -\dfrac{j}{\omega C_{as4}} \\ -\dfrac{j}{\omega C_{as4}} & j\omega L - \dfrac{j}{\omega C_{as4}} \end{bmatrix}. \quad (8)$$

Then, the value of equivalent elements can be calculated as

$$L_{as4} = \frac{\operatorname{Im}\left(Z_{11}^{A4}\right) - \operatorname{Im}\left(Z_{12}^{A4}\right)}{2\pi f_0}, \qquad C_{as4} = -\frac{1}{2\pi f_0 \operatorname{Im}\left(Z_{12}^{A4}\right)}. \quad (9)$$

For interdigital capacitor Aj ($j = 1, 2$) as shown in Figure 4(e), its admittance matrix can be expressed by

Table 1: Detailed element parameters of ATLs.

70.7 Ω	L_{as1}	L_{as2}	L_{as3}	L_{as4}	C_{as1}	C_{as2}	C_{as3}	C_{as4}
	3.56 nH	0.97 nH	2.33 nH	2.01 nH	0.34 pF	0.41 pF	0.39 pF	0.46 pF
	C_{ap1}	C_{ap2}	C_{a11}	C_{a12}	C_{a21}	C_{a22}		
	0.24 pF	0.99 pF	0.09 pF	0.12 pF	0.34 pF	0.41 pF		
50 Ω	L_{bs1}	L_{bs2}	L_{bs3}	L_{bs4}	L_{bs5}	C_{bs1}	C_{bs2}	C_{bs3}
	2.46 nH	1.31 nH	1.01 nH	1.02 nH	1.18 nH	0.79 pF	0.51 pF	0.72 pF
	C_{bs4}	C_{bp1}	C_{bp2}	C_{b11}	C_{b12}	C_{b21}	C_{b22}	
	0.32 pF	0.42 pF	0.51 pF	0.19 pF	0.19 pF	0.24 pF	0.25 pF	
35.4 Ω	L_{cs1}	L_{cs2}	L_{cs3}	L_{cs4}	L_{cs5}	C_{cs1}	C_{cs2}	C_{cs3}
	1.52 nH	0.33 nH	0.78 nH	0.91 nH	1.01 nH	1.75 pF	0.51 pF	0.83 pF
	C_{cs4}	C_{cp1}	C_{cp2}	C_{c11}	C_{c12}	C_{c21}	C_{c22}	
	0.62 pF	0.95 pF	0.19 pF	0.42 pF	0.41 pF	0.11 pF	0.14 pF	

$$\begin{bmatrix} Y_{11}^{\text{int } j} & Y_{12}^{\text{int } j} \\ Y_{21}^{\text{int } j} & Y_{22}^{\text{int } j} \end{bmatrix} = \begin{bmatrix} j\omega C_{aj1} + j\omega C_{apj} & -j\omega C_{apj} \\ -j\omega C_{apj} & j\omega C_{aj2} + j\omega C_{apj} \end{bmatrix}. \tag{10}$$

Then, the equivalent capacitance value can be calculated by

$$\begin{aligned} C_{apj} &= -\frac{\text{Im}\left(Y_{12}^{\text{int } j}\right)}{2\pi f_0}, \\ C_{aj1} &= \frac{\text{Im}\left(Y_{11}^{\text{int } j}\right) + \text{Im}\left(Y_{12}^{\text{int } j}\right)}{2\pi f_0}, \\ C_{aj2} &= \frac{\text{Im}\left(Y_{22}^{\text{int } j}\right) + \text{Im}\left(Y_{12}^{\text{int } j}\right)}{2\pi f_0}. \end{aligned} \tag{11}$$

All values of equivalent elements as marked in Figures 1(b), 2(b), and 3(b) are given in Table 1.

The final optimized size of ATLs used in the proposed Wilkinson power divider and branch-line coupler are listed in Table 2 as marked in Figures 1(a), 2(a), and 3(a). The physical lengths of the 70.7 Ω, 50 Ω, and 35.4 Ω ATLs are $0.098\lambda_g$, $0.104\lambda_g$, and $0.124\lambda_g$, respectively.

2.3. Harmonic Suppression. For the proposed ATLs, the interdigital capacitors can play a role of harmonic suppression. For the interdigital capacitors, the performance of harmonic suppression is mainly determined by the number, length, width of finger, and gap width between fingers [24]. In order to realize the compact size and easy fabrication, the gap width between fingers is chosen to be 0.2 mm. Then, other factors affecting harmonic suppression would be discussed.

Taking the 70.7 Ω ATL mentioned above as an example, the interdigital capacitors have 19 fingers and the length $L_{a6} = 5.2$ mm and width $W_{a6} = 0.2$ mm as marked in Figure 1(a). The 70.7 Ω ATLs with different fingers' numbers, lengths, and widths of interdigital capacitors are simulated.

When the fingers' number of interdigital capacitors changes, while their length $L_{a6} = 5.2$ mm and width $W_{a6} = 0.2$ mm remain unchanged, the simulated $|S_{21}|$ are shown in Figure 5(a). It can be observed that when the fingers' number is reduced, the frequency of transmission zero in stopband becomes higher. In addition, compared to the ATL without interdigital capacitors, the ATL with interdigital capacitors has obvious harmonic suppression. The influence of fingers' length on harmonic suppression is given in Figure 5(b). When the number of fingers equals to 19 and fingers' width $W_{a6} = 0.2$ mm, it can be seen that the frequency of transmission zero becomes higher as fingers' length is shortened. Figure 5(c) reveals that the frequency of transmission zero varies as fingers' width W_{a6} changes when the interdigital capacitors have 7 fingers with 5.2 mm length. When fingers' width increases, the frequency of transmission zero would be lower slightly.

The result of such simulations is because the reduction of fingers' number, length, and width would reduce the capacitance of C_{ap1} and C_{ap2}. The reduced capacitance of C_{ap1} and C_{ap2} would make the resonant frequency of the parallel resonant circuit higher, which is composed of C_{ap1}, C_{ap2}, and L_{as4}. And the resonant frequency is the frequency of transmission zero in a stopband, so the harmonic suppression is affected.

2.4. Propagation Characteristics. All of these proposed ATLs are designed to operate at 0.9 GHz and with 90° phase delay. The layout of ATLs are simulated by the electromagnetic simulation solver of IE3D, while their corresponding equivalent lumped circuits as given in Figures 1(b), 2(b) and 3(b) are simulated by software of ADS. The comparisons of simulated *S*-parameters between the layout and equivalent lumped circuit are given in Figure 6. Additionally, when the 70.7 Ω, 50 Ω and 35.4 Ω ATLs are simulated, the reference impedances of the ports are set to 70.7 Ω, 50 Ω, and 35.4 Ω, respectively.

As shown in Figure 6(a), for the 70.7 Ω ATL, the simulated *S*-parameters show that it has a 152.2% bandwidth of 0.9 GHz, from 0 GHz to 1.37 GHz. At 0.9 GHz, the return loss is 45.63 dB while insertion loss is less than

Table 2: Optimized dimensions of ATLs (unit: mm).

70.7 Ω	L_{a1}	L_{a2}	L_{a3}	L_{a4}	L_{a5}	L_{a6}	W_{a1}	W_{a2}	W_{a3}	W_{a4}	W_{a5}	W_{a6}	W_{a7}
	22.2	2.3	6.9	11.7	21.6	5.2	5.4	0.2	1.7	1.7	0.7	0.2	0.2
50 Ω	L_{b1}	L_{b2}	L_{b3}	L_{b4}	L_{b5}	W_{b1}	W_{b2}	W_{b3}	W_{b4}	W_{b5}	W_{b6}	W_{b7}	W_{b8}
	23.4	5.8	12.1	15.2	22.6	3.8	4	0.6	0.3	0.3	2.9	0.3	0.4
35.4 Ω	L_{c1}	L_{c2}	L_{c3}	L_{c4}	W_{c1}	W_{c2}	W_{c3}	W_{c4}	W_{c5}	W_{c6}	W_{c7}	W_{c8}	
	28.6	12.7	16.1	27	6.4	6.6	0.2	0.2	4.6	4.7	2	0.5	

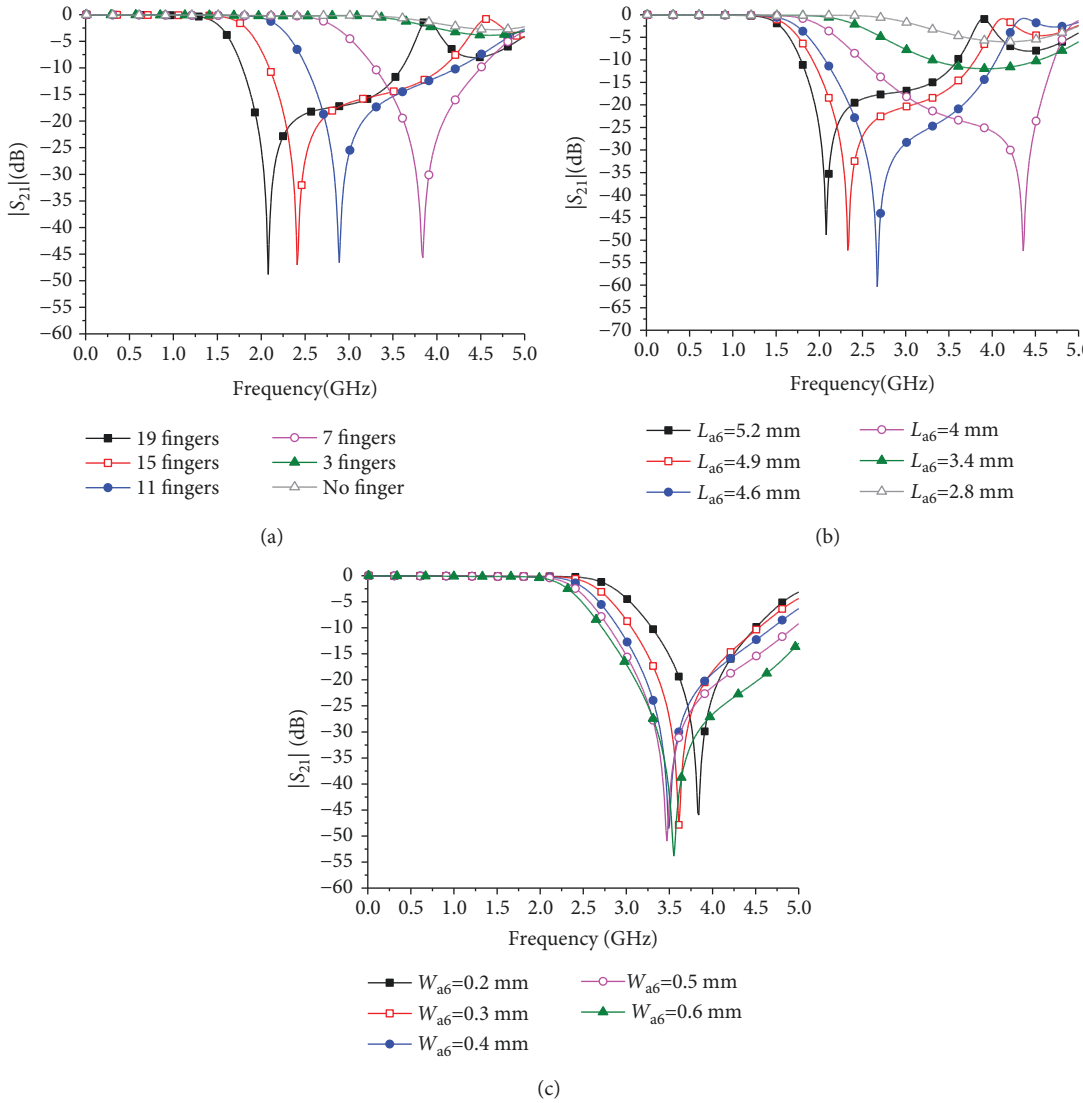

Figure 5: Harmonic suppression of the 70.7 Ω ATL: (a) different number, (b) different length, and (c) different width.

0.1 dB. Moreover, harmonic suppression performance is also shown in Figure 6(a). For the second-order harmonic frequency at 1.8 GHz, $|S_{21}|$ is -10.66 dB, while for the third-order harmonic frequency at 2.7 GHz, $|S_{21}|$ is -17.71 dB. For these harmonic frequencies, there are no pass-bands.

For 50 Ω ATL as shown in Figure 6(b), the layout simulation displays a 170% bandwidth of 0.9 GHz, from 0 GHz to 1.53 GHz. At 0.9 GHz, the ATL achieves 39.56 dB return loss and insertion loss less than 0.1 dB. Moreover, its harmonic suppression performance is verified by 12.5 dB harmonic suppression at the third-order harmonic frequency at 2.7 GHz.

For the 35.4 Ω ATL as exhibited in Figure 6(c), it has a 161.1% bandwidth of 0.9 GHz, from 0 GHz to 1.45 GHz. When operating at 0.9 GHz, 52.7 dB return loss and less than

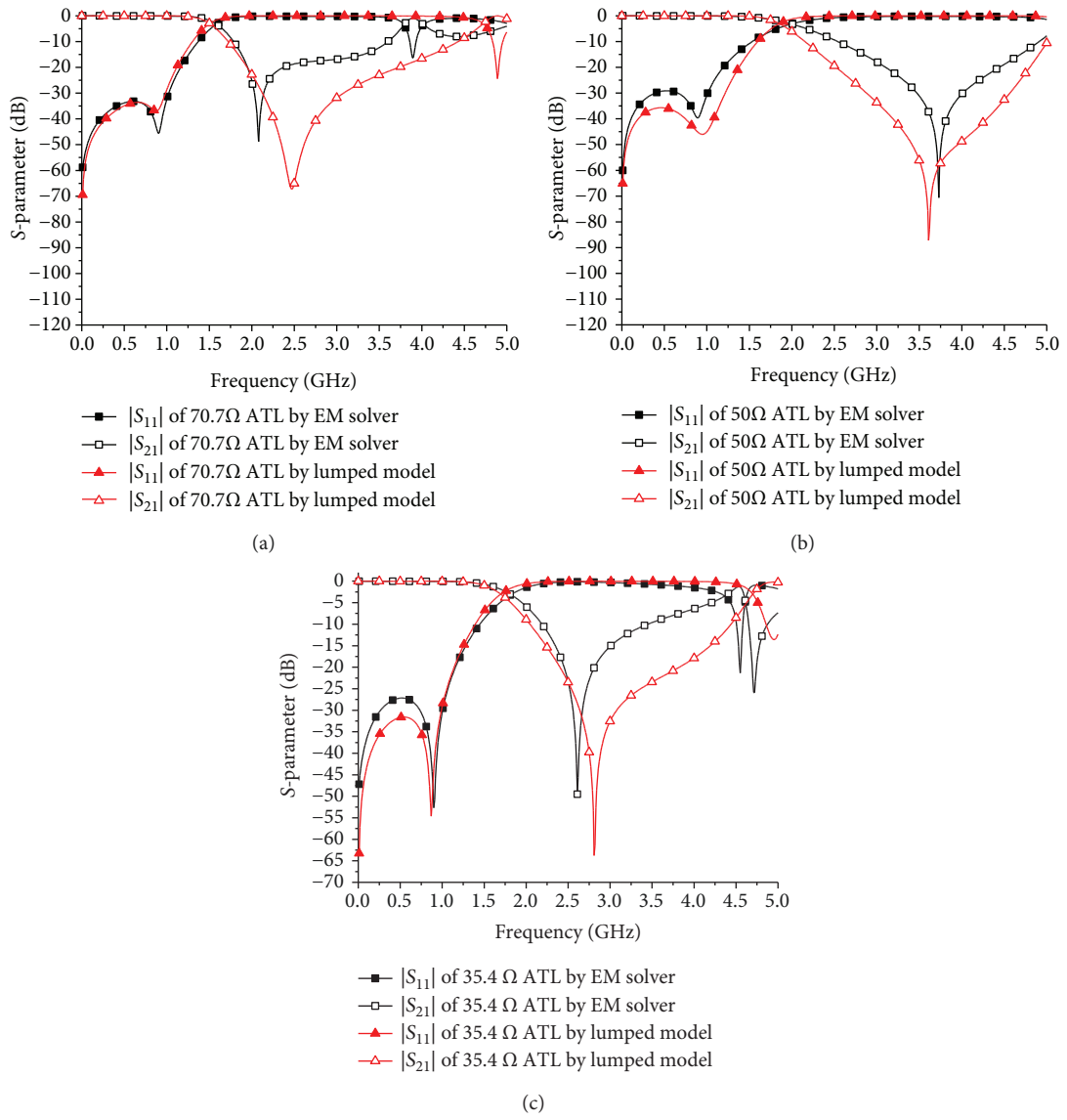

Figure 6: Simulated *S*-parameter of the proposed ATLs: (a) 70.7 Ω, (b) 50 Ω, and (c) 35.4 Ω.

0.1 dB insertion loss are realized. For the 35.4 Ω ATL, the third-order harmonic is suppressed to 26.63 dB, which displays good harmonic suppression performance.

The simulated characteristic impedance and phase delay are exhibited in Figures 7 and 8. For the 70.7 Ω ATL, at 0.9 GHz, the real part of characteristic impedance is 70.7 Ω and the imaginary part is 0.42 Ω, while the simulated results of the equivalent circuit are 70.93 Ω and 2.08 Ω. For the 50 Ω ATL, the 50.0 Ω real part and -0.56 Ω imaginary part of characteristic impedance can be obtained, while the results of equivalent circuit simulation are 50.5 Ω and -0.1 Ω. For the 35.4Ω ATL, the real part of characteristic impedance is 35.4 Ω and the imaginary part is 0.24 Ω, while the corresponding results of the equivalent circuit are 35.85 Ω and -0.15 Ω.

Figure 8 indicates that the 70.7 Ω ATL has 90.0° phase delay at 0.9 GHz while 90.13° for the equivalent circuit. The 50 Ω ATL has 90.0° phase delay at 0.9 GHz while 91.52° for the equivalent circuit. The 35.4 Ω ATL has 90.1° phase delay and 91.15° for the equivalent circuit.

From the analysis above, these proposed ATLs not only have the similar performance like conventional transmission lines within the bandwidth but also have effective suppression ability for the harmonics. For the ATLs, the simulated *S*-parameters of the layout agree well with that of the lumped equivalent circuit at low frequency. However, at high frequency, there is a deviation of insertion losses, due to the equivalent circuit of the interdigital capacitor. In addition, the precision of the equivalent circuit would be improved by dividing the interdigital capacitor into more numbers of equivalent series capacitors. The simulation comparisons between the layout and lumped model indicate the accuracy of extracting parameters of the equivalent circuit.

3. Circuit Design and Measurements

The proposed Wilkinson power divider and branch-line coupler are designed to operate at 0.9 GHz. Simulations are performed by a full-wave EM simulation software of IE3D. The

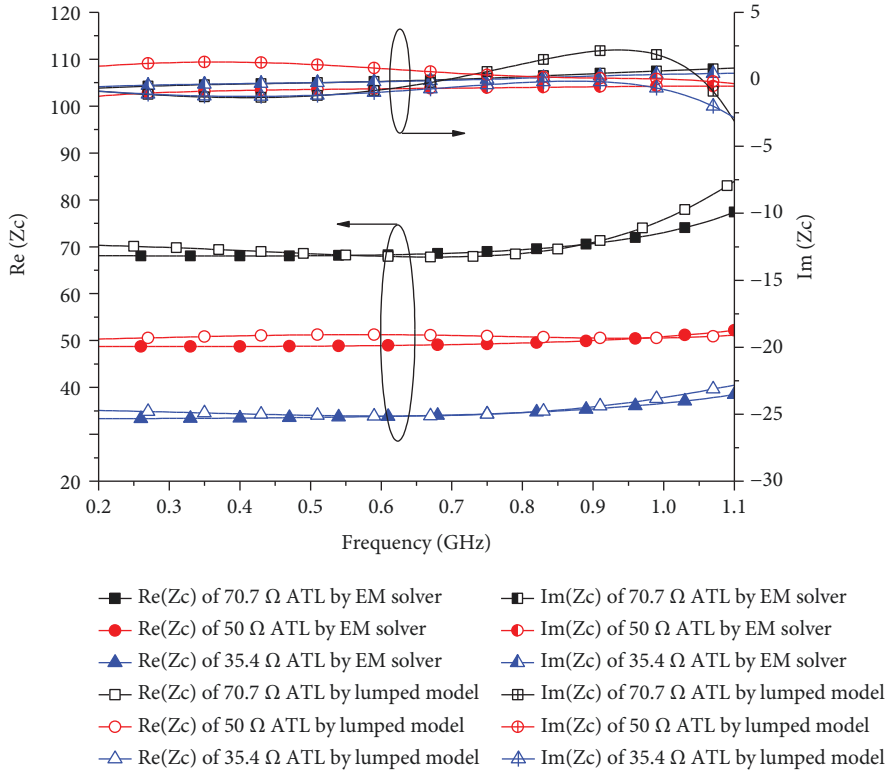

Figure 7: Simulated characteristic impedance of the proposed ATLs.

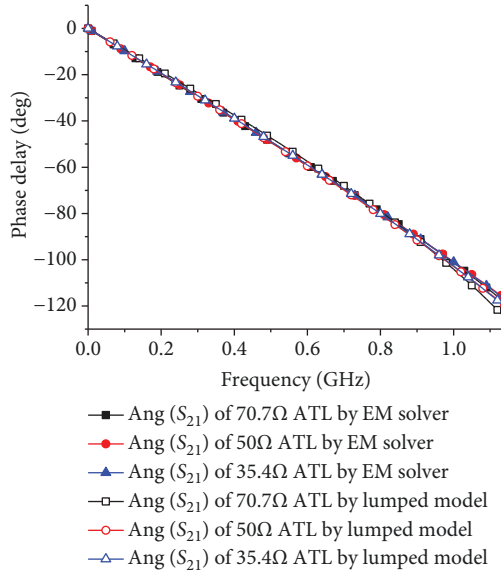

Figure 8: Simulated phase delay of the proposed ATLs.

proposed Wilkinson power divider and branch-line coupler are fabricated on a substrate of F4B with 1 mm thickness and relative permittivity $\varepsilon_r = 2.65$ and loss tangent $\delta = 0.005$. Measurements are carried out on an Agilent 8510C network analyzer.

3.1. Wilkinson Power Divider. The layout of proposed Wilkinson power divider is given by Figure 9(a). The proposed Wilkinson power divider consists of two sections of 70.7 Ω ATLs employed to replace these conventional quarter-wavelength transmission lines. And a chip resistor of 100 Ω (type: 0805) is used in the design. The photograph of the fabricated Wilkinson power divider is shown in Figure 9(b). The proposed Wilkinson power divider occupies a size of 29.9 mm × 34.7 mm, that is $0.13\lambda_g \times 0.16\lambda_g$, where λ_g is the guided wavelength on the substrate at 0.9 GHz.

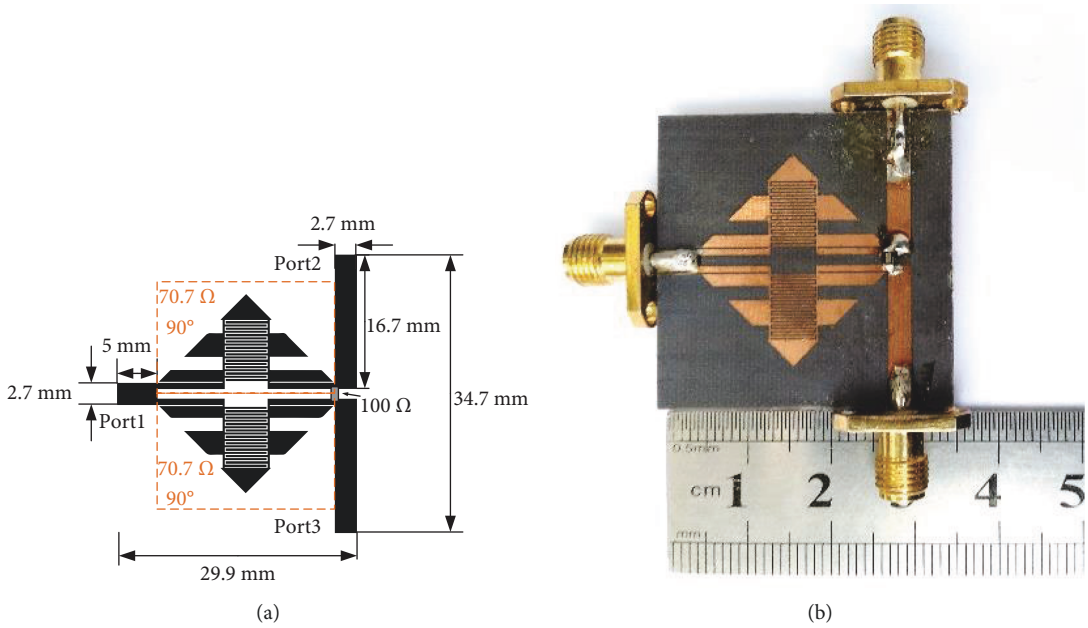

FIGURE 9: The proposed Wilkinson power divider: (a) layout and (b) photo.

Comparing to a power divider implemented by conventional microstrip lines, the fabricated power divider only occupies a 58.8% size.

Figure 10 shows the simulated and measured $|S_{11}|$, $|S_{21}|$, and $|S_{31}|$ of the proposed Wilkinson power divider. The simulated and measured S-parameters indicate that the measured results have a good agreement with simulated results. For simulation, the central frequency is 0.9 GHz while measurements exhibit the central frequency of 0.91 GHz. There exists a frequency deviation of 0.01 GHz for central frequency due to fabrication tolerance and measurement devices. Then, the fabricated Wilkinson power divider for 0.91GHz has a bandwidth of 58.2% for $|S_{11}|$ less than -15 dB, from 0.61 GHz to 1.14 GHz, and the return loss at 0.91 GHz is 32.12 dB. At 0.91GHz, measured $|S_{21}|$ is -3.13 dB and $|S_{31}|$ is -3.26 dB. In addition, as shown in Figure 10, the fabricated Wilkinson power divider has 12.5 dB suppression for the second-order harmonic of 1.82 GHz and 24.7 dB suppression for the third-order harmonic of 2.73 GHz.

Figure 11 shows isolation and phase difference (Ang(S_{21})-Ang(S_{31})). Measured results display at 0.91 GHz that the power divider has a 32.8 dB isolation, which reveals good isolation performance between output port 2 and port 3. Besides, there is only a 0.23° phase difference between two output port 2 and port 3 at 0.91 GHz.

Figure 12 gives the comparison of S-parameters between the proposed Wilkinson power divider and conventional case operating at 0.9 GHz, which obviously indicates that the harmonic is effectively suppressed in the stopband in the proposed structure. Meanwhile, a similar bandwidth performance as that of the conventional case is achieved when size miniaturization is realized.

Finally, the performance comparisons of this proposed power divider (this work) with several previous designs are

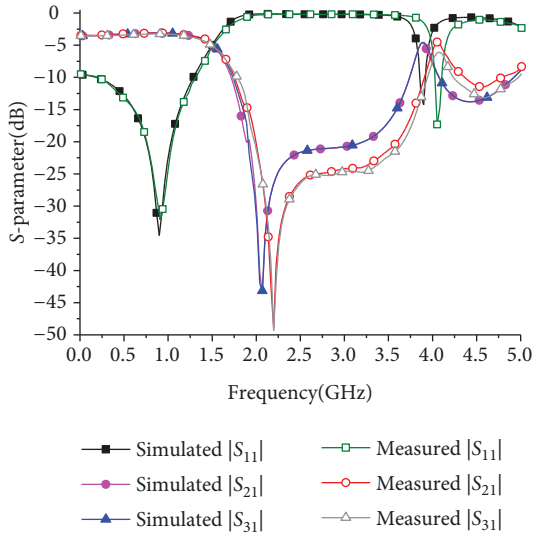

FIGURE 10: Simulated and measured $|S_{11}|$, $|S_{21}|$, and $|S_{31}|$ of the proposed Wilkinson power divider.

listed in Table 3. It indicates the proposed Wilkinson power divider in this work has similar electrical performance as the conventional case and good harmonic suppression but with a small size. Especially, the relative bandwidth is similar to the conventional one.

3.2. Branch-Line Coupler. In the design of the proposed 3 dB branch-line coupler as shown in Figure 13(a), two sections of 50 Ω ATLs and two sections of 35.4 Ω ATLs are employed to replace these corresponding conventional quarter-wavelength transmission lines. The two sections of 50 Ω ATLs are designed to be with a right-angled triangle

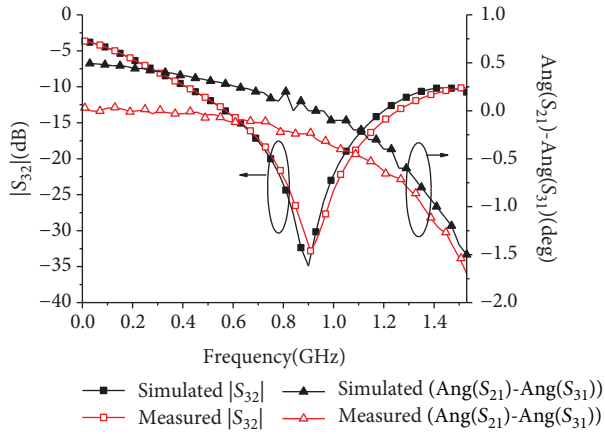

Figure 11: Simulated and measured $|S_{32}|$ and phase difference of the proposed Wilkinson power divider.

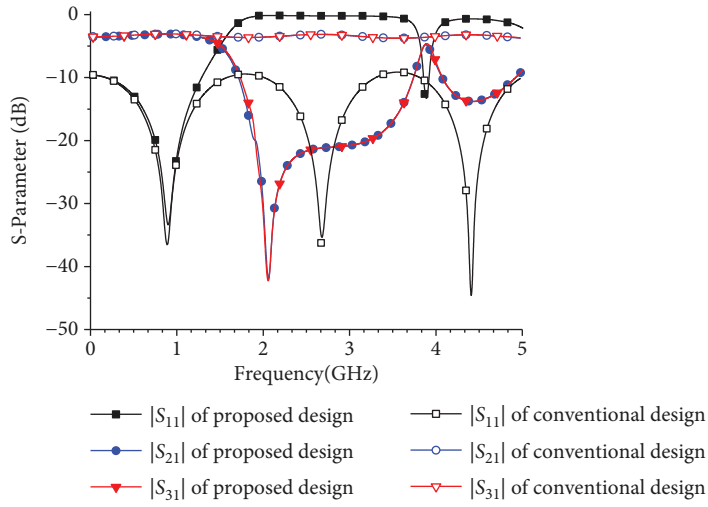

Figure 12: Comparison of simulated S-parameters between the proposed and conventional Wilkinson power divider.

Table 3: Performance comparisons of power dividers.

Ref	Central frequency (GHz)	Size	$\lvert S_{11}\rvert$ -15 dB BW (%)	At central frequency			Harmonic suppression (dB)	
				$\lvert S_{11}\rvert$ (dB)	$\lvert S_{21}\rvert$, $\lvert S_{31}\rvert$ (dB)	$\lvert S_{32}\rvert$ (dB)	Second-order harmonic	Third-order harmonic
[15]	0.9	$0.1\lambda_g \times 0.2\lambda_g$	2.4	15	4.74 ± 0.15	23	27	36
[16]	0.9	$0.11\lambda_g \times 0.15\lambda_g$	4.5	16	4.6, 4.6	30	47	45
[17]	0.92	$0.15\lambda_g \times 0.14\lambda_g$	6.5	22	3.96, 3.99	20	45	No given
[18]	0.9	$0.11\lambda_g \times 0.06\lambda_g$	21.1	25	3.5, 3.6	19	5	41
[25]	0.77	$0.042\lambda_g \times 0.189\lambda_g$	38	20	3.52, 3.52	20.8	40	37
[26]	2.4	$0.17\lambda_g \times 0.1\lambda_g$	69	50	3.4, 3.5	33	No suppression	No suppression
This work	0.91	$0.13\lambda_g \times 0.16\lambda_g$	58.2	32.12	3.13, 3.26	32.8	12.5	24.7

λ_g: guided wavelength at central frequency.

shape, while the two sections of 35.4 Ω ATLs are modified to an isosceles trapezoid shape in order to realize a more compact size. All of these ATLs are combined into a compact rectangle shape. The photograph of the fabricated 3 dB branch-line coupler is given in Figure 13(b). The size of the fabricated branch-line coupler is 45.2 mm × 32.8

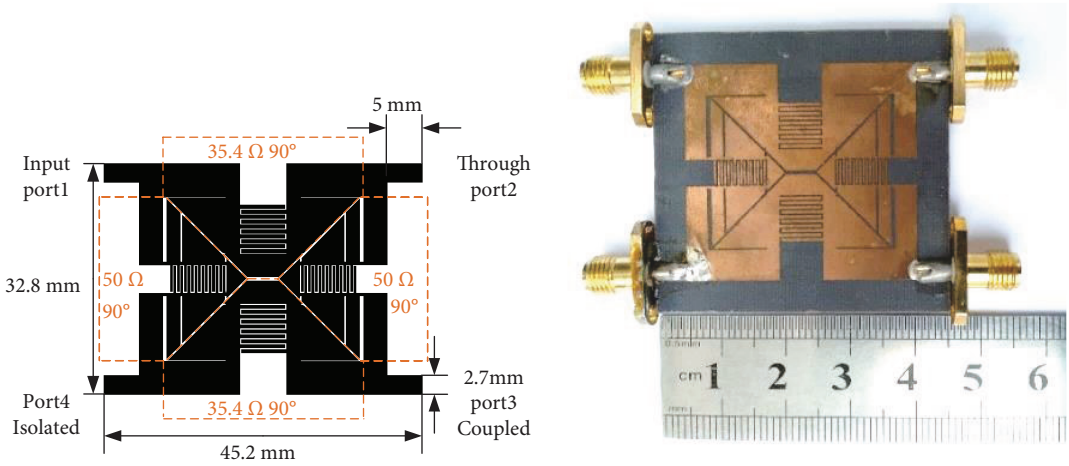

Figure 13: The proposed 3 dB branch-line coupler: (a) layout and (b) photo.

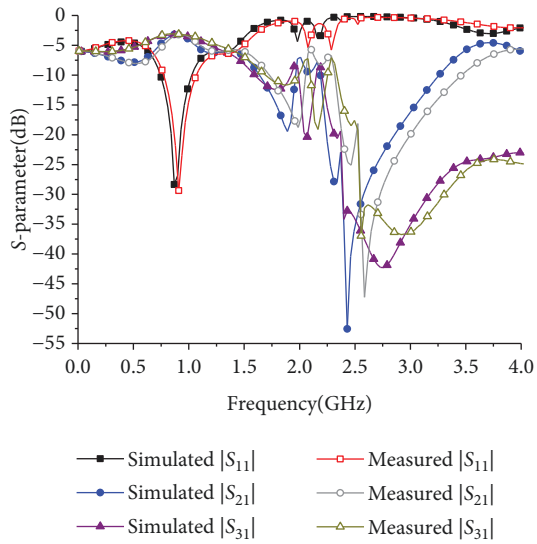

Figure 14: Simulated and measured $|S_{11}|$, $|S_{21}|$, and $|S_{31}|$ of the proposed branch-line coupler.

mm, that is $0.2\lambda_g \times 0.15\lambda_g$, where λ_g is the guided wavelength on the substrate at 0.9 GHz. The size of the proposed branch-line coupler is effectively reduced to a 33.4% area of a conventional one at 0.9 GHz.

Figure 14 shows the simulated and measured $|S_{11}|$, $|S_{21}|$, and $|S_{31}|$ of the proposed coupler. The S-parameters reveal a good agreement between simulated and measured results. As observed in Figure 14, the central frequency is 0.9 GHz at simulation while the central frequency is 0.91 GHz at measurement. A frequency deviation of 0.01 GHz exists between simulation and measurement because of fabrication tolerance and measurement devices. For measured results, at a central frequency of 0.91 GHz, it has a 17% bandwidth with $|S_{11}|$ less than -15 dB, from 0.84 GHz to 0.99 GHz. At 0.91 GHz, the return loss is 29.35 dB, which shows its good impedance match with ports. And at 0.91 GHz, $|S_{21}|$ and $|S_{31}|$ are -3.2 dB and -3.15 dB, respectively. In Figure 15, $|S_{41}|$ and phase difference between the two output ports are given. At 0.91 GHz, measured $|S_{41}|$ is -26.3 dB. The phase difference (Ang(S_{21})-Ang(S_{31})) is 90.6°, while the 90° ± 1° bandwidth is 34 MHz, from 881 MHz to 915 MHz.

In addition, at the second-order harmonic frequency of 1.82 GHz, $|S_{11}|$ is -1.26 dB, $|S_{21}|$ is -12.6 dB, and $|S_{31}|$ is -11.1 dB. At the third-order harmonic frequency of 2.73 GHz, $|S_{11}|$ is -0.34 dB, $|S_{21}|$ is -29.5 dB, $|S_{31}|$ is -33.9 dB. It is demonstrated that at the second-order and third-order harmonic frequencies, there are no pass-bands. So harmonic suppression performance is verified. As a comparison, S-parameters of the conventional branch-line coupler are given in Figure 16. By observation, the bandwidth of the proposed branch-coupler is comparable to that of the conventional one, while these harmonic pass-bands at harmonic frequencies are effectively suppressed.

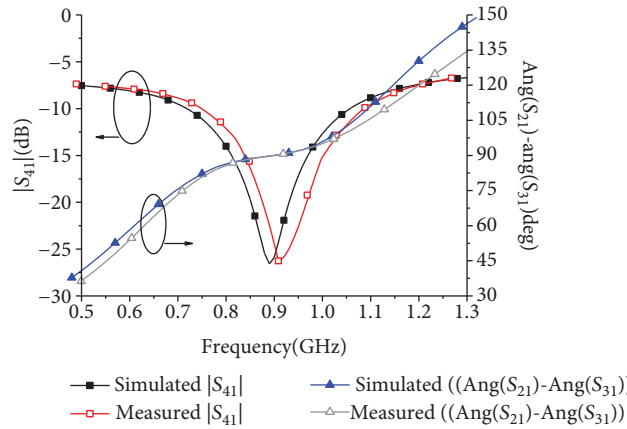

Figure 15: Simulated and measured $|S_{41}|$ and phase difference of the proposed branch-line coupler.

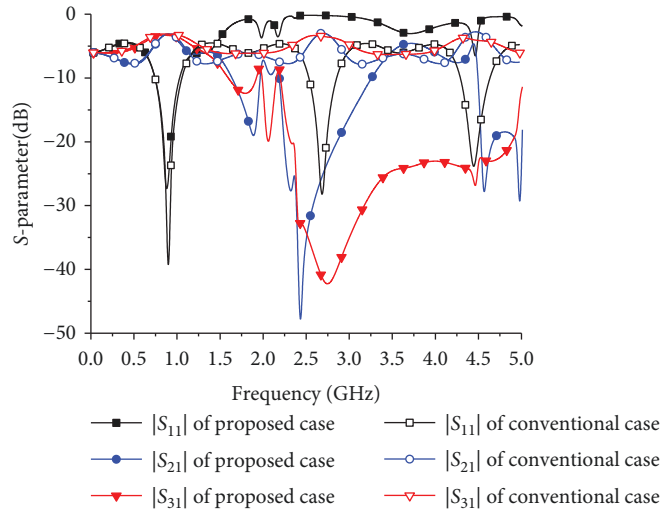

Figure 16: Simulated *S*-parameters of the conventional branch-line coupler.

Table 4: Performance comparisons of branch-line couplers.

Ref	Central frequency (GHz)	Size	$\|S_{11}\|$ -15 dB BW (%)	At central frequency			Harmonic suppression (dB)	
				$\|S_{11}\|$ (dB)	$\|S_{21}\|$, $\|S_{31}\|$ (dB)	$\|S_{41}\|$ (dB)	Second-order harmonic	Third-order harmonic
[19]	0.91	$0.09\lambda_g \times 0.11\lambda_g$	8.9	33	3.2, 3.7	40	No suppression	No suppression
[20]	0.9	$0.07\lambda_g \times 0.11\lambda_g$	18.9	30	3.36, 3.25	22	No suppression	No suppression
[21]	0.8365	$0.08\lambda_g \times 0.07\lambda_g$	7.2	25	3.9, 3.9	28.9	20	No given
[22]	0.875	$0.10\lambda_g \times 0.11\lambda_g$	19.4	35	2.94, 3.72	43	5	5
[27]	1	$0.19\lambda_g \times 0.34\lambda_g$	20	34	3.5, 3.6	30	No suppression	No suppression
[28]	1.675	$0.16\lambda_g \times 0.16\lambda_g$	23.2	35.1	2.8, 3.15	34.1	No suppression	No suppression
This work	0.91	$0.2\lambda_g \times 0.15\lambda_g$	17	29.35	3.2, 3.15	26.3	12.6	29.5

λ_g: guided wavelength at central frequency.

Table 4 shows the performance comparisons of the proposed branch-line coupler (this work) and several previous designs. The performance comparisons reveal that the proposed branch-line coupler has similar bandwidth, insertion loss, and isolation with other designs, but better harmonic suppression with a miniaturized size.

4. Conclusion

In this paper, a compact Wilkinson power divider and a compact 3 dB branch-line coupler with harmonic suppression performance based on artificial transmission lines are proposed. These ATLs consist of stepped impedance transmission lines and interdigital capacitors. In order to reduce the size, these ATLs are folded into a right-angled triangle shape, and especially, the 35.4 Ω ATLs employed in the branch-line coupler are modified to an isosceles trapezoid shape. Then, the feasibility of the proposed power divider and branch-line coupler design are demonstrated, and the simulated and the measured results are in good agreement. The proposed Wilkinson power divider realizes the 58.8% occupied area of the conventional case and good harmonic suppression performance. The occupied area of the proposed branch-line coupler is reduced to 33.4% of the conventional case. At the same time, good harmonic suppression performance is demonstrated. Both proposed components have similar bandwidth as the conventional design but with compact size and good harmonic suppression. The proposed Wilkinson power divider and branch-line coupler can be extensively used in the modern communication system.

Data Availability

All data included in this study are available from the corresponding author upon request.

Conflicts of Interest

The authors declare that there are no conflicts of interest.

Acknowledgments

This work was supported by the Chongqing Research Program of Basic Research and Frontier Technology (cstc2017jcyjAX0128), the Chongqing Postgraduate Innovative Research Project (CYS18243), and the National Natural Science Foundation of China (61401054).

References

[1] S. Kumar and D. K. Vishwakarma, "Miniaturisation of microstrip patch antenna using an artificial planar magneto-dielectric meta-substrate," *IET Microwaves, Antennas & Propagation*, vol. 10, no. 11, pp. 1235–1241, 2016.

[2] D. Psychogiou, R. Gómez-García, A. C. Guyette, and D. Peroulis, "Reconfigurable single/multi-band filtering power divider based on quasi-bandpass sections," *IEEE Microwave and Wireless Components Letters*, vol. 26, no. 9, pp. 684–686, 2016.

[3] L. Chang and T. G. Ma, "Dual-mode branch-line/rat-race coupler using composite right-/left-handed lines," *IEEE Microwave and Wireless Components Letters*, vol. 27, no. 5, pp. 449–451, 2017.

[4] Y. Zheng and W. Sheng, "Compact lumped-element LTCC bandpass filter for low-loss VHF-band applications," *IEEE Microwave and Wireless Components Letters*, vol. 27, no. 12, pp. 1074–1076, 2017.

[5] B. F. Zong, G. M. Wang, Y. W. Wang, L. Geng, and D. Wang, "Compact antenna using finger-connected interdigital capacitor-based composite right/left-handed transmission-line unit cell," *IEEE Transactions on Antennas and Propagation*, vol. 64, no. 5, pp. 1994–1999, 2016.

[6] P. R. Prajapati, G. G. K. Murthy, A. Patnaik, and M. V. Kartikeyan, "Design and testing of a compact circularly polarised microstrip antenna with fractal defected ground structure for L-band applications," *IET Microwaves, Antennas & Propagation*, vol. 9, no. 11, pp. 1179–1185, 2015.

[7] A. Y. I. Ashyap, Z. Z. Abidin, S. H. Dahlan et al., "Compact and low-profile textile EBG-based antenna for wearable medical applications," *IEEE Antennas and Wireless Propagation Letters*, vol. 16, pp. 2550–2553, 2017.

[8] J. Selga, P. Vélez, J. Coromina, A. Fernández-Prieto, J. Bonache, and F. Martín, "Harmonic suppression in branch-line couplers based on slow-wave transmission lines with simultaneous inductive and capacitive loading," *Microwave and Optical Technology Letters*, vol. 60, pp. 2374–2384, 2018.

[9] F.-X. Liu, Y. Wang, X. Y. Zhang, C. H. Quan, and J. C. Lee, "A size-reduced tri-band Gysel power divider with ultra-wideband harmonics suppression performance," *IEEE Access*, vol. 6, pp. 34198–34205, 2018.

[10] Q. S. Shen, M. J. Gao, L. S. Wu, and X. L. Zhou, "Ultra-wideband filtering 180° hybrid coupler with super wide upper stopband using swap phase inverter and electromagnetic bandgap structures on double-sided parallel-strip line," *IEEE Access*, vol. 6, pp. 41099–41106, 2018.

[11] Z. Qamar, S. Y. Zheng, W. S. Chan, and D. Ho, "Coupling coefficient reconfigurable wideband branch-line coupler topology with harmonic suppression," *IEEE Transactions on Microwave Theory and Techniques*, vol. 66, no. 4, pp. 1912–1920, 2018.

[12] L. Li, J. F. Mao, M. Tang, and H. Dai, "Mixed-mode property of defected ground structure and its application in balanced network design with harmonic suppression," *IEEE Microwave and Wireless Components Letters*, vol. 28, no. 3, pp. 188–190, 2018.

[13] J. Selga, J. Coromina, P. Vélez et al., "Compact power splitter with harmonic suppression based on inductively-loaded slow-wave transmission lines," *Microwave and Optical Technology Letters*, vol. 60, no. 6, pp. 1464–1468, 2018.

[14] R. K. Singh, A. Basu, and S. K. Koul, "A novel pattern-reconfigurable oscillating active integrated antenna," *IEEE Antennas and Wireless Propagation Letters*, vol. 16, pp. 3220–3223, 2017.

[15] W. M. Chau, K. W. Hsu, and W. H. Tu, "Filter-based Wilkinson power divider," *IEEE Microwave and Wireless Components Letters*, vol. 24, no. 4, pp. 239–241, 2014.

[16] C.-F. Chen, T.-Y. Huang, T.-M. Shen, T.-M. Shen, and R.-B. Wu, "Design of miniaturized filtering power dividers for system-in-a-package," *IEEE Transactions on Components, Packaging and Manufacturing Technology*, vol. 3, no. 10, pp. 1663–1672, 2013.

[17] X. Y. Zhang, K. X. Wang, and B. J. Hu, "Compact filtering power divider with enhanced second-harmonic suppression," *IEEE Microwave and Wireless Components Letters*, vol. 23, no. 9, pp. 483–485, 2013.

[18] C. C. Chen, C. Y. D. Sim, J. W. Chen, and J. H. Lin, "Miniaturised Wilkinson power divider with wide-stopband using

synthetic transmission line," *Electronics Letters*, vol. 53, no. 15, pp. 1056–1058, 2017.

[19] C. H. Tseng and C. H. Wu, "Design of compact branch-line couplers using π-equivalent artificial transmission lines," *IET Microwaves, Antennas & Propagation*, vol. 6, no. 9, pp. 969–974, 2012.

[20] C. H. Tseng and C. L. Chang, "A rigorous design methodology for compact planar branch-line and rat-race couplers with asymmetrical T-structures," *IEEE Transactions on Microwave Theory and Techniques*, vol. 60, no. 7, pp. 2085–2092, 2012.

[21] K. Y. Tsai, H. S. Yang, J. H. Chen, and Y. J. E. Chen, "A miniaturized 3 dB branch-line hybrid coupler with harmonics suppression," *IEEE Microwave and Wireless Components Letters*, vol. 21, no. 10, pp. 537–539, 2011.

[22] B. F. Zong, G. M. Wang, C. X. Zhang, and Y. W. Wang, "Miniaturised branch-line coupler with ultra-wide high suppression stopband," *Electronics Letters*, vol. 50, no. 19, pp. 1365–1367, 2014.

[23] A. Abdipour, A. Abdipour, and E. Zare, "A design of branch-line coupler with harmonic suppression and size reduction using closed-loop and open-loop resonators," *Radioengineering*, vol. 26, no. 4, pp. 999–1005, 2017.

[24] J. S. Hong and M. J. Lancaster, *Microstrip Filters for RF/Microwave Applications*, John Wiley, New York, NY, USA, 2001.

[25] G. Shen, W. Che, Q. Xue, and W. Feng, "Novel design of miniaturized filtering power dividers using dual-composite right-/left-handed resonators," *IEEE Transactions on Microwave Theory and Techniques*, vol. 66, no. 12, pp. 5260–5271, 2018.

[26] N. al-Areqi, K. Y. You, C. Y. Lee, N. H. Khamis, and M. N. Dimon, "Wideband and compact Wilkinson power divider utilizing series delta-stub and folded stepped-impedance transmission line," *Radioengineering*, vol. 27, no. 1, pp. 200–206, 2018.

[27] S. Reshma and M. K. Mandal, "Miniaturization of a 90° hybrid coupler with improved bandwidth performance," *IEEE Microwave and Wireless Components Letters*, vol. 26, no. 11, pp. 891–893, 2016.

[28] L. Sun, Y. Z. Yin, X. Lei, and V. Wong, "A novel miniaturized branch-line coupler with equivalent transmission lines," *Progress In Electromagnetics Research Letters*, vol. 38, pp. 35–44, 2013.

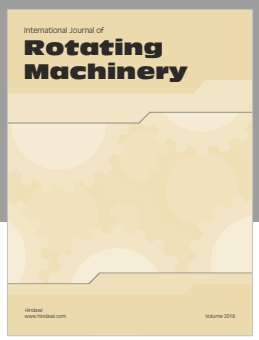

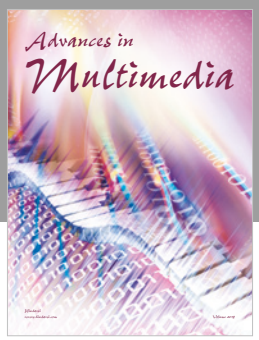

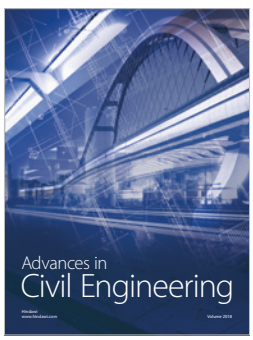

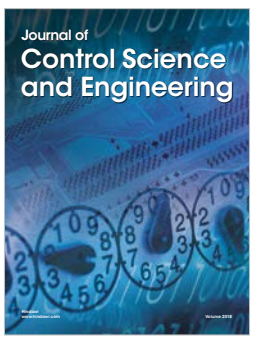

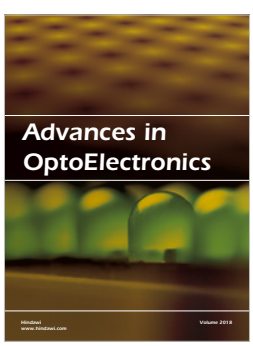

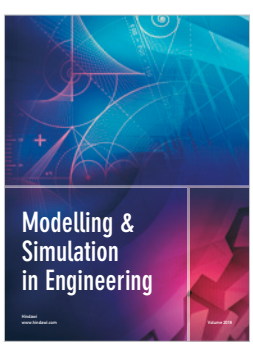

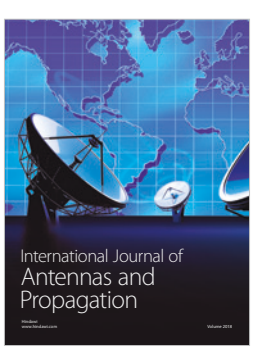

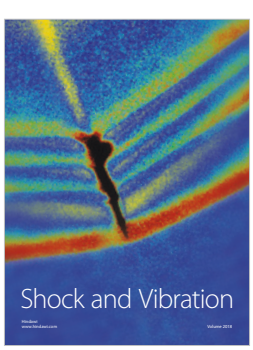

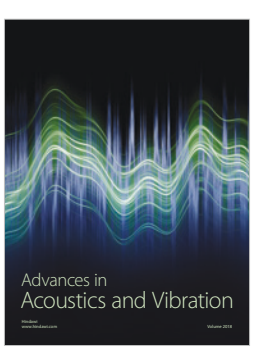

Hindawi

Submit your manuscripts at
www.hindawi.com